Available online at www.sciencedirect.com
SCIENCE DIRECT
Carbohydrate Polymers 60 (2005) 475–481
Carbohydrate Polymers
www.elsevier.com/locate/carbpol

Solution properties of starch nanoparticles in water and DMSO as studied by dynamic light scattering

Soma Chakraborty[1], Bishwabhusan Sahoo, Iwao Teraoka*, Richard A. Gross

NSF Center for Biocatalysis and Bioprocessing of Macromolecules, Polytechnic University, Six Metrotech Center, Brooklyn, NY 11201, USA

Received 8 January 2004; accepted 3 March 2005
Available online 28 April 2005

Abstract

Solution properties of starch nanoparticles dispersed in DMSO and in water were studied using dynamic light scattering. The particle size distribution had two main peaks in both solvents at all scattering angles studied. They were at around 40 and 300 nm, ascribed to isolated starch nanoparticles and their aggregates, respectively. From the excess scattering intensity by the 40-nm particles, the molecular weight of the nanoparticle was estimated as $2.2–2.6\times10^6$ g/mol. When the concentration was increased, another peak appeared at around 1 μm. Raising the temperature from 25 to 65 °C did not change the distribution, indicating a purely entropic process in dynamic equilibrium of the aggregation. In DMSO, an oscillatory behavior was observed in the autocorrelation function at high temperatures.

Keywords: Starch; Amylopectin; Nanoparticles; Dynamic light scattering; Particle size distribution; Aggregation

1. Introduction

Starch is a biocompatible, biodegradable, nontoxic polymer, existing in nature as the major storage polysaccharide in higher plants. Native starches are a blend of two polyglucans, amylose and amylopectin. Amylose is the linear fraction consisting of α-D-glucose linked through α (1→4) linkages and has a molecular weight of $10^5–10^6$ g/mol (Wesslén & Wesslén, 2002). Amylopectins, with molecular weights between 10^6 and 10^7 g/mol, are branched fractions containing short chains linking linear chains via α (1→6) linkages. Starch is being used in a broad range of applications as a thickener, stabilizer, gelling agent and a drug carrier (Bayazeed, Elzairy, & Hebeish, 1989; Jeffcoat, Mason, Emling, & Chiu, 2002; Lind, Kresse, Debus, & Muller, 2002; Ragheb, El-Sayiad, & Hebeish, 1997; Schmidt, Herald, & Khatib, 2001; Whaley, Kasica, Senkeleski, Foss, & Heigis, 1999). The first step in these applications, especially for drug delivery, is to disperse each starch molecule in solvents such as water and dimethyl sulfoxide (DMSO) in non-degradative conditions. Typically, it is accomplished by swelling starch in dried DMSO, followed by mixing with water (Radosta, Haberer, & Vorwerg, 2001). An alternative way is through generating lightly cross-linked starch nanoparticles. The potential of starch nanoparticles and microspheres as drug carriers has been extensively studied (Brigger, Dubernet, & Couvreur, 2002; Illum, Fisher, Jabbat & Davis, 2001; Debuigne, Cuisenaire, Jeunieau, Masereel, & Nagy, 2001).

The present paper reports solution properties of the starch nanoparticles in DMSO and water. We took advantage of spectral decomposition of dynamic light scattering to investigate the shape, molecular weight and other natures of the starch nanoparticles. Our findings will tell whether these starch nanoparticles meet the criteria required for drug delivery applications. Solution properties of starch molecules dispersed in DMSO, water and aqueous DMSO, have been extensively investigated using static and dynamic light scattering (DLS) (Kapoor & Bhattacharya, 2000; Ring, I'Anson, & Morris, 1985; Roger, Bello-Perez, & Colonna, 1999), but so far studies on solution properties of starch nanoparticles have not been documented.

* Corresponding author. Tel.: +1 718 2603 466; fax: +1 718 2603 125.
E-mail address: teraoka@poly.edu (I. Teraoka).
[1] Present address: Department of Chemical Engineering, Columbia University, New York, NY 10027, USA.

0144-8617/$ - see front matter © 2005 Elsevier Ltd. All rights reserved.
doi:10.1016/j.carbpol.2005.03.011

2. Materials and methods

2.1. Materials

Starch nanoparticles were a gift from Ecosynthetix (Lansing, MI). According to the manufacturer, waxy corn starch with glycerol (18 wt% of dry starch) as plasticiser and glyoxal (0.1–10 wt%) as crosslinker was fed to an extruder (Berstorff ZE40) and extruded with a screw speed at 160 rpm. Granules obtained from the extrusion were cryogenically ground and sieved to obtain particles smaller than 150 nm in diameter.

DMSO was purchased from Aldrich. Water was deionised using a RiOs™16 water purification system (Millipore). Deionized water was passed through a Milli-Q® Ultrapure water purification system (Millipore) where combination of UV irradiation, ion exchange and ultrafiltration was used to remove particles, organic matter and bacteria.

2.2. Dynamic light scattering measurement

Particle size distribution of starch nanoparticles was characterized by using a N4 Plus Particle Sizer (Beckman-Coulter) with a He–Ne laser (wavelength $\lambda = 632.8$ nm; 10 mW) as a light source. Samples for the measurement were prepared by dissolving nanoparticles in DMSO or water. DMSO solutions were filtered through a hydrophobic PTFE filter, and aqueous solutions through a hydrophilic PTFE filter (both 0.2 μm pore size; Millipore), unless otherwise mentioned. Filtered solutions were collected into dust-free fluorometer cells (10×10 mm). The measurements were conducted at 25 °C unless otherwise specified. N4 Plus measures the autocorrelation function of light scattering intensity and converts it into a distribution of the apparent particle diameter d, assuming that the light scattering comes from spherical particles independently making diffusional motion. The conversion uses CONTIN, an inverse-Laplace transform program package (Provencher, 1982). The Stokes–Einstein relationship gives d as

$$d = \frac{k_B T}{(3\pi\eta D)} \quad (1)$$

where k_B is the Boltzmann constant, T the temperature, η the solvent viscosity and D the diffusion coefficient. The apparent hydrodynamic radius R_H is equal to $d/2$. The distribution of d is weighted by the scattering intensity of each particle of the relevant size at the scattering angle used. N4 Plus has six scattering angles from 10 to 90°. The actual scattering angle depends slightly on the refractive index n of the solvent. Since the data at the lowest angle (10°) were not reliable, they were not used for further analysis.

The viscosity data of water and DMSO at different temperatures were taken from a reference (Viswanath & Natarajan, 1989): $\log_{10}[\eta/(\text{Pa s})] = A + B/(C - T/K)$ with $A = -4.5318$, $B = -220.57$, $C = 149.39$ for water and $A = -4.3585$, $B = -323.95$, $C = 102.62$ for DMSO. Data supplied with the N4 Plus was used for the refractive index of water at different temperatures. For DMSO, we estimated the index at different temperatures using $n = 1.477$ at 20 °C and $dn/dT = -0.0004\ K^{-1}$. This formula is not exact, but the associated error in the estimate of d is negligible compared with other errors.

3. Results

3.1. Autocorrelation functions and size distributions

Fig. 1 shows the baseline-subtracted, normalized autocorrelation function $g_2(t)$ of light scattering intensity as a function of delay time t measured at $\theta = 90$, 62.6, 30.2, 23° for a 1.00% (w/w) aqueous solution of starch nanoparticles. Two traces of $g_2(t)$ are shown at each angle. The $g_2(t)$ at different angles nearly overlap each other when plotted as a function of k^2t, where $k = (4\pi n/\lambda)\sin(\theta/2)$ is the scattering wave vector (not shown). The latter result indicates diffusional behavior of the nanoparticles. Similar results were obtained for starch nanoparticles dispersed in DMSO.

A typical size distribution of starch nanoparticles calculated from $g_2(t)$ is shown in Fig. 2. Two peaks are prominent at around 50 and 300 nm. There is another small peak at around 2 nm. The smaller of the diameters for the two prominent peaks is close to the diameter (~40 nm) estimated in the manufacturer-supplied scanning electron micrograph of dried nanoparticles. Therefore, the peak at 50 nm is assigned mostly to isolated 40 nm nanoparticles. The peak at 300 nm can be ascribed to their aggregates. The position of the 300-nm peak moves to a smaller diameter with an increasing scattering angle θ, indicating that aggregates have a size distribution. The relative area of the peak at 50 nm increases with an

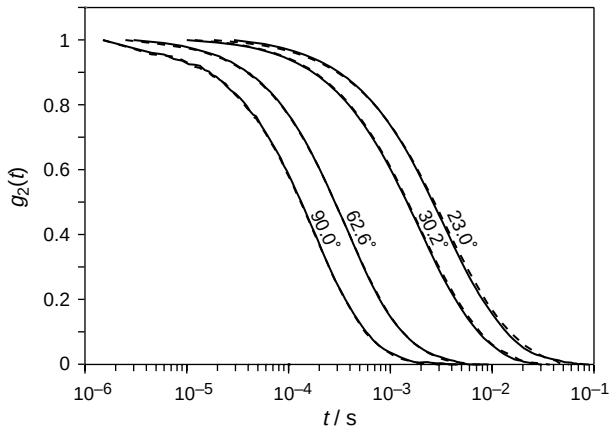

Fig. 1. Baseline-subtracted, normalized intensity autocorrelation function $g_2(t)$, plotted as a function of delay time t for a 1.00% (w/w) aqueous solution of starch nanoparticles at 25 °C. The scattering angles are, from left to right, 90, 62.6, 30.2, and 23°. Two traces are shown as a solid line and a dashed line at each scattering angle.

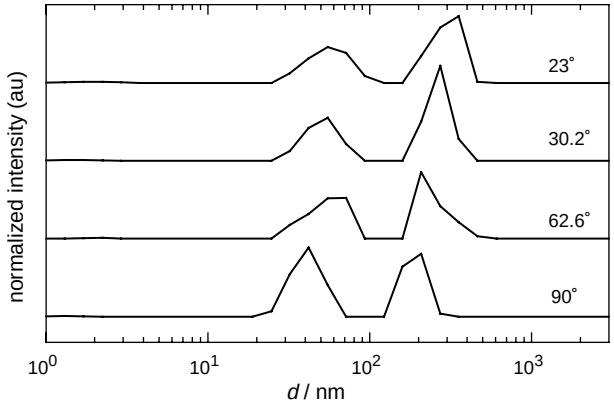

Fig. 2. Particle size distribution of starch nanoparticles in 1.00% (w/w) solution in water at 25 °C, measured at four scattering angles indicated adjacent to the curves.

increasing θ. The run-to-run variation in the peak area ratio is less than 10%.

The distribution also exhibits three peaks in DMSO as shown in Fig. 3. The diameter for isolated particles is slightly smaller (40 nm or less), but the diameter for the aggregates is almost identical to the one observed in water at each θ. The position of the 40-nm peak barely moves with θ. The change of the relative areas of the two major peaks with θ is similar to the one observed in water. The third peak at around 2 nm is more visible than it is in Fig. 2.

3.2. Unfiltered solutions

Although not desirable for light scattering experiments, we also conducted DLS measurements for unfiltered solutions in water and DMSO. To minimize complications from dust particles, the solutions were left undisturbed in a cuvette for at least 4 days prior to the measurements. The autocorrelation functions were much more scattered for the unfiltered solutions, especially at low angles. Fig. 4 shows typical particle size distributions at four scattering angles for the aqueous solution. The area ratio of the 300–40-nm

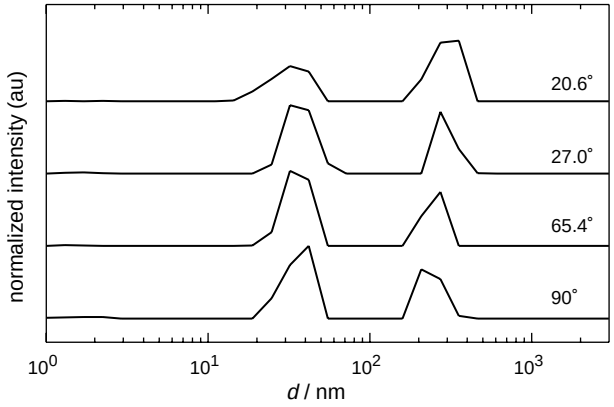

Fig. 3. Particle size distribution of starch nanoparticles in 1.00% (w/w) solution in DMSO at 25 °C, measured at four scattering angles.

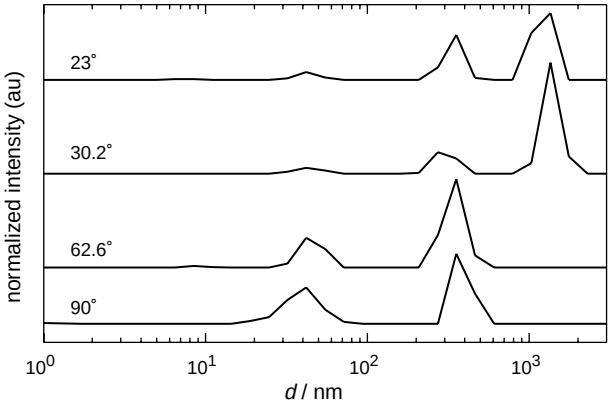

Fig. 4. Particle size distribution of starch nanoparticles in unfiltered 1.00% (w/w) solution in water at 25 °C, measured at four scattering angles.

peak is much greater compared with the unfiltered solutions, especially at low angles. In addition to these peaks, a large peak at around 1.3 μm is observed at low angles. The results were similar for unfiltered solutions in DMSO. The absence of the 1.3-μm peak in the filtered solutions indicates either that the filtration removed the permanent aggregates or that the particles that passed the filter have less tendency to form the large dynamic aggregates.

The product of the total excess scattering intensity and the area fraction of each peak in the distribution curve gives the scattering intensity by the particles of that size. The scattering intensities by the 40 and 300-nm particles were thus calculated at each scattering angle for filtered and unfiltered solutions in water and DMSO. We then compared the intensity before and after filtration for each of the two sizes at different angles (not shown). The 300-nm particles show a large decrease in the intensity by filtration. The decrease is different from angle to angle, since the intensity includes the one by the 1.3-μm particles when CONTIN failed to separate the 300-nm and 1.3-μm peak. In contrast, 40-nm particles show a consistent trend. In both solvents, the intensities before and after the filtration are identical within experimental errors that are less than 10% at all angles. Apparently, isolated nanoparticles were not retained by the filter.

To find whether the 300-nm peak is ascribed to dynamic aggregates that are in equilibrium with isolated 40-nm particles, a starch nanoparticle solution in water was filtered through an Anodisc membrane filter (0.02 μm; Whatman). The presence of starch was verified by dropping an iodine solution into the filtered sample. DLS analysis of the filtered sample showed three peaks (2, 50, and 300 nm) whose positions were the same as those of the samples filtered through the 0.2-μm filter. Their photon counts were also comparable, confirming that the peak at 300 nm in Fig. 2 is due to formation of dynamic aggregates.

3.3. Concentration effect

Fig. 5 compares the size distribution for four concentrations of aqueous solution (filtered). The aggregation is

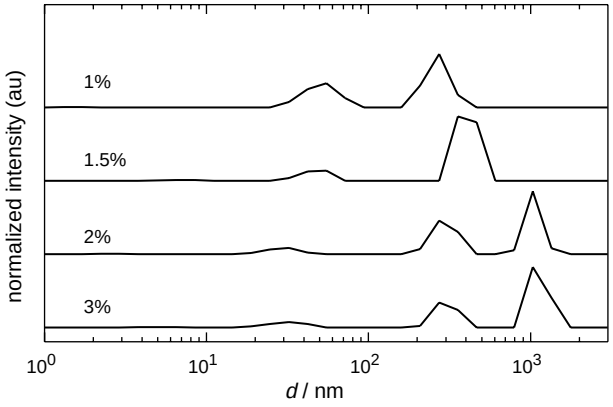

Fig. 5. Particle size distribution of starch nanoparticles in aqueous solutions at different concentrations, measured at $\theta = 30.2°$. The concentration (w/w) is indicated adjacent to each curve.

more obvious at higher concentrations. Another large peak appears at around 1 μm when the concentration of starch nanoparticles in water is 2% (w/w) or higher. Note that these large aggregates were formed after filtration through a 0.2-μm filter.

3.4. Temperature effect

When the temperature was increased from 25 to 65 °C, there was little change in the peak positions of the size distribution in water (Fig. 6). Apparently, the aqueous dispersions are stable at least up to 65 °C. The distribution at 25 °C in Fig. 6 is different from the one for $\theta = 30.2°$ in Fig. 2; the temperature dependence was studied after the solution had been left in a refrigerator for two months before filtration. A larger area for the 300-nm peak in Fig. 6 may indicate a slow growth of aggregates in the refrigerator.

Temperature dependence was also studied for the nanoparticles in DMSO. Unlike aqueous solutions, the autocorrelation functions at higher temperatures were different from those at low temperatures. Fig. 7 compares

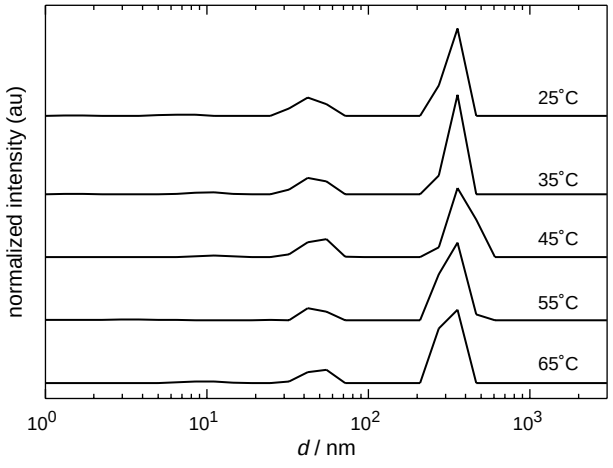

Fig. 6. Particle size distribution of starch nanoparticles in 1.00% (w/w) solution in water at different temperatures, measured at $\theta = 30.2°$.

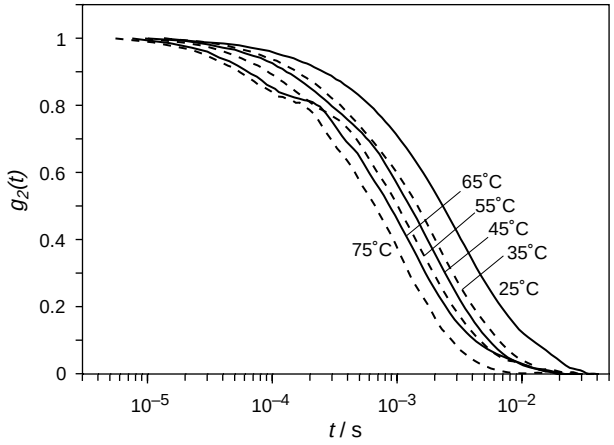

Fig. 7. Baseline-subtracted, normalized autocorrelation function $g_2(t)$, plotted as a function of delay time t for a 1.00% (w/w) solution of starch nanoparticles in DMSO, measured at $\theta = 30°$. The temperatures are, from right to left, 25, 35, 45, 55, 65, and 75 °C. Solid and dashed lines are used alternately to distinguish the lines.

the autocorrelation function ($\theta = 30.2°$) at 25, 35, 45, 55, 65, and 75 °C. With an increasing temperature, the plot shifts to left because the less viscous solvent and the k_BT factor make the diffusion faster. A deviation from the sigmoidal decay is evident at 65 and 75 °C, and to a lesser extent at 45 and 55 °C. A similar deviation with the same characteristic time was observed at the tail portion of the autocorrelation function at $\theta = 90°$ and in the middle portion of the function at $\theta = 62.6°$. The characteristic time of the deviation (inflection point to the left of the shoulder in $g_2(t)$) is around 0.1 ms at 75 °C. The deviation moves to a longer time and becomes less visible at a lower temperature. Another deviation from the sigmoidal decay with a longer characteristic time was also observed at low angles (not shown). Its characteristic time is around 0.06 s at 75 °C and shifts to a longer time and becomes less visible with decreasing temperature. In water, in contrast, the autocorrelation functions were diffusional at all the temperatures and scattering angles studied. The absence of oscillatory behavior in aqueous solutions and the low optical absorption of the starch nanoparticles and DMSO precludes convection (Schaertl & Roos, 1999) as the cause of the observed oscillatory behavior in DMSO.

4. Discussion

4.1. Molecular weight of nanoparticles

Here, we assume that the mass concentration of the nanoparticles did not change by filtration and use the excess scattering intensity I_{ex} obtained for the filtered 1% solutions to estimate the molecular weight M of the 40-nm particle. Here, I_{ex} refers to the excess scattering intensity times the area fraction of the 40-nm peak in the size distribution. We note that the 300-nm particles have only a small fraction of

mass, as will be shown in Section 4.2. Therefore, the mass concentration of the 40-nm particles is nearly equal to the overall mass concentration. We do the estimation for water and DMSO separately. This type of analysis would be impossible without the spectral decomposition capability of DLS. Angular dependence of the total I_{ex} alone would give a wrong estimate.

The following equation relates M to I_{ex} obtained for different macromolecules in solutions of different concentrations (in dilute regime) in different solvents at a given scattering angle

$$\frac{1}{M} \propto \left(\frac{c}{I_{ex}}\right)\left(n\frac{dn}{dc}\right)^2 \quad (2)$$

where c is the concentration (mass/volume) of the molecules, and dn/dc is the specific refractive index increment. Starch in water has $dn/dc = 0.151$ ml/g (Roger & Colonna, 1992).

The data of I_{ex} were corrected for the angle-dependent scattering volume (due to different pinhole sizes in N4 Plus) using the photon count data obtained for a dilute suspension of polystyrene latex 25 nm radius. It was assumed that the latter scatters light according to the Rayleigh–Gans formula.

The proportionality constant in Eq. (2) was determined for polystyrene beads of $R_H = 50$ nm (nominal) dispersed in water. A dispersion of 8.3×10^{-6} g/ml was used. We approximated its dn/dc by the refractive index difference between polystyrene (1.595) and water (1.333) divided by the density of bulk polystyrene (1.05 g/ml) (Teraoka, 2002). Different readings of I_{ex} at angles from 23 to 90° for the starch nanoparticle solution in water resulted in $2.2–2.6\times10^6$ g/mol for M. The uncertainty in this estimate comes mostly from the errors in the area fraction.

Together with $d = 50$ nm in water, the fiber density of starch in the nanoparticles is estimated as 0.06 g/cm^3. This value indicates that the particles are highly porous.

Starch in DMSO has $dn/dc = 0.0659$ ml/g (Everett & Foster, 1959). In DMSO, I_{ex} at 90° is less reliable compared with lower angles because of a weaker scattering. We used the data at 65.4–20.6° to obtain $1.7–2.2\times10^6$ g/mol for M in DMSO. Together with $d = 40$ nm, The fiber density is estimated as 0.12 g/cm^3. The greater diameter of isolated nanoparticles in water compared with DMSO indicates that they swell more in water.

Now that each nanoparticle is essentially a small container housing starch in the semidilute regime, the third weak peak at around 2 nm in water and DMSO is ascribed to the cooperative diffusion mode of entangled or cross-linked chains. The correlation length is 2 nm, which is not necessarily identical to the mean distance between adjacent cross-linking points. The cross-linking is needed to maintain structural integrity, but entanglement can occur at much higher densities. The correlation length of 2 nm agrees with the one observed in other cross-linked polymeric gels in the swollen state at around the same fiber fraction (Amis, Jammey, Ferry, & Yu, 1983; Munch, Candau, Herz, & Hild, 1977; Shibayama, 1998).

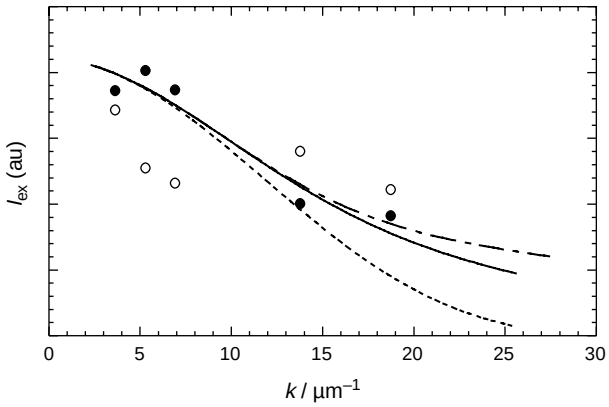

Fig. 8. Excess scattering intensity I_{ex} by 40-nm particles (open circles) and 300-nm particles (closed circles) in 1.00% (w/w) solution of starch nanoparticles in water, plotted as a function of the scattering vector k. Also shown is the form factor of a solid sphere 140 nm radius as a dashed line, the factor of a Gaussian chain ($R_g = 108$ nm) as a solid line, and the factor of a rod 374-nm long as a dash-dotted line.

4.2. Conformation of the aggregates

Now we use the component I_{ex} in the excess scattering for the 300-nm particles to find their conformation. Filled circles in Fig. 8 show the component as a function of the scattering vector k for the aqueous solution. For the 40-nm particles I_{ex} is flat, except for the lowest-angle data, whereas I_{ex} for the 300-nm particles falls off with an increasing k, a reasonable result since the aggregate size is comparable to the laser wavelength λ, whereas $40\text{ nm} \ll \lambda$.

The plot of I_{ex} for the 300-nm particles can be used to estimate its radius of gyration R_g. The data of $I_{ex}(0)/I_{ex}(\theta)$ at 23, 30.2, and 62.6° were fitted with $I_{ex}(0)/I_{ex}(\theta) = 1 + (1/3)R_g^2k^2$ for the estimation. The procedure is independent of the shape or conformation of the particles. The fitting gives $R_g = 108$ nm in water. For this value of R_g, $\theta = 62.6°$ does not qualify as a sufficiently low angle for the fitting. However, the error caused by that is rather small, as will be discussed later.

The estimate of R_g gives $R_H/R_g = 1.4$, close to 1.29, the value for a solid sphere. In contrast, a random coil of a Gaussian conformation has $R_H/R_g = 0.67$ (excluded-volume chain has a similar value) (Teraoka, 2002). Thus, we can conclude that the aggregates are not chain-like or extended, but rather take a compact shape.

Using the R_g value obtained, we plot in Fig. 8 the form factor, $I_{ex}(\theta)/I_{ex}(0)$, for three typical shapes of the aggregates: a solid sphere of radius 140 nm ($=(5/3)^{1/2}\times R_g$), a random-coil chain of the particles (Gaussian-chain conformation with $R_g = 180$ nm), and a rod of length $(12)^{1/2}R_g$. Note that a distribution in the particle size makes the decrease in the three curves less sharp. The comparison of the three curves alone with the experimental data cannot tell which conformation

best describes the shape of the aggregates. However, it does not preclude the solid-sphere conformation either. For more detailed discussion, we need to take an average from a lot more data on decomposed I_{ex}. The small difference between the three curves at $k=13.8\ \mu m^{-1}$ ($\theta=62.6°$) justifies our including the 62.6° data for the estimation of R_g.

If we assume a solid sphere for the conformation of the 300-nm particles, their population is extremely small. The mass fraction of the 300-nm particles is less than 0.003 in water. The number will not be much different in DMSO.

The quality of the data for DMSO solutions was not sufficiently good for reliable estimation of R_g for the 300-nm particles. The weaker refractive index contrast compared with the aqueous solutions and the freezing point of DMSO close to room temperature resulted in a greater run-to-run variation in the area fractions of the two main peaks and a greater sample-to-sample variation in the total scattering intensity. Further studies are needed.

4.3. Aggregation equilibrium

The presence of the 300-nm aggregates in diameter can be explained on the basis of the open association model (Young, Brigault, Heenan, Higgins, & Peiffer, 1998). The model assumes dynamic equilibrium between aggregates of different sizes. Specifically, an aggregate consisting of i particles, M_i, gains another particle, $M=M_1$, to become M_{i+1}

$$M_i + M \leftrightarrow M_{i+1} \tag{3}$$

where $i=1, 2,\ldots$

We assume that the equilibrium constant $K_{eq}=[M_{i+1}]/[M_i][M]$ is independent of i, and $[M]$ changes little during the equilibration. The latter assumption is reasonable when the particles are predominantly present as isolated particles as in our starch nanoparticle dispersions. Then the model gives a distribution of $[M_i]$ identical to the one for the degree of polymerization (most probable distribution or exponential distribution) to be obtained in stepwise addition mechanisms such as polycondensation of bifunctional monomers. When these aggregates are observed in light scattering, the scattering by M_i is weighted by i^2 at low scattering angles, and therefore, the scattering intensity of M_i exhibits a peak at around the mass average of M_i. A greater K_{eq} will let the peak appear at a greater i. The peak shifts to smaller i with an increasing scattering angle, since the weight factor becomes less than i^2. The exponential distribution itself does not have a peak. The peak in the size distribution we observed is solely due to the weight factor.

Of course, the assumption of i-independent K_{eq} is too simplistic. A more realistic assumption may be that $K_{eq} \propto i$; a larger aggregate has more sites to add another nanoparticle. In fact, the latter explains better the angular dependence of the apparent particle diameter of the aggregate than the i-independent K_{eq} does.

4.4. Concentration effect

The appearance of the 1-μm peak in 2 and 3% solutions in water despite filtration through a 0.2-μm filter indicates that it is due to dynamic agglomerates. Increasing the concentration resulted in the appearance of another peak at 1 μm, not the shift of the peak position for the 300-nm particle. The aggregation equilibrium described by Eq. (3) holds independently of concentration, as it should be. Rather it appears that the nanoparticle solution has a hierarchy of association: Some of the 300-nm aggregates associate into a larger agglomerate.

4.5. Temperature effect

The size of the aggregate in water does not change with temperature (Fig. 6). It means that K_{eq} is independent of temperature T. We note that $K_{eq} \propto \exp[-\Delta H/RT + \Delta S/R]$, where R is the gas constant, ΔH and ΔS are the molar enthalpy change and the molar entropy change of each reaction in Eq. (3). The temperature independence of K_{eq} leads to $\Delta H \cong 0$. The aggregate formation is governed by ΔS. A much greater population of isolated nanoparticles indicates that $\Delta S/R$ is negative and $-\Delta S/R \gg 1$.

The oscillatory behavior in $g_2(t)$ in Fig. 7 is ascribed to the chain reactions in Eq. (3). If the kinetic equation consisted only of a single i, i.e. $iM \leftrightarrow M_i$, then the oscillatory behavior would not be seen. Rather, a faster decay constant would be observed (Schmitz, 1990). The oscillatory behavior needs at least two reactions of different i in Eq. (3).

5. Conclusions

We used dynamic light scattering to characterize starch nanoparticles in water and DMSO. In both solvents, the particle size distribution showed two peaks at around 40 and 300 nm. The smaller particles were identified as isolated particles, whereas the larger particles were ascribed to their aggregates with a compact shape. Spectral decomposition capability of dynamic light scattering allowed us to estimate the molecular weight of each nanoparticle.

Acknowledgements

We acknowledge financial support to S. Chakraborty from through the NSF Industry-University Cooperative Research Center for Biocatalysis and Bioprocessing of Macromolecules. We thank M. Noto for sharing the data on polystyrene latex with us.

References

Amis, E. J., Jammey, P. A., Ferry, J. D., & Yu, H. (1983). Quasielastic light scattering for gelatin solutions and gels. *Macromolecules*, *16*, 441–446.

Bayazeed, A., Elzairy, M. R., & Hebeish, A. (1989). Synthesis and applications of new thickners. Part 1: Preparation of poly(acrylic acid)-starch graft copolymer. *Starch/Stärke*, *41*, 233–236.

Brigger, I., Dubernet, C., & Couvreur, P. (2002). Nanoparticles in cancer therapy. *Advanced Drug Delivery Reviews*, *54*, 631–651.

Debuigne, F., Cuisenaire, L., Jeunieau, L., Masereel, B., & Nagy, J. B. (2001). Synthesis of nimesulide nanoparticles in the microemulsion of epikuran/isopropyl myristate/water/*n*-butanol (or isopropanol). *Journal of Colloid Interface Science*, *243*, 90–101.

Everett, W. W., & Foster, J. F. (1959). The subfraction of amylose and characterization of the subfractions by light scattering. *Journal of the American Chemistry Society*, *81*, 3459–3464.

Illum, L., Fisher, A. N., Jabbat Gill, I., & Davis, S. S. (2001). Bioadhesive starch microsphere and absorption enhancing agents act synergistically to enhance the nasal absorption of polypeotides. *International Journal of Pharmaceutics*, *222*, 109–119.

Jeffcoat, R., Mason, W. R., Emling, J. L., & Chiu, C.-W. (2002). Stabilized crosslinked waxy potato starch as food additive. European Patent EP, 1229049, 15pp.

Kapoor, B., & Bhattacharya, M. (2000). Dynamic and extensional properties of starch in aqueous dimethyl sulfoxide. *Carbohydrate Polymers*, *42*, 323–335.

Lind, K., Kresse, M., Debus, N. P., & Muller, R. H. (2002). A novel formulation for superparamagnetic iron oxide (SPIO) particles enhancing MR lymphograph: Comparison of physiochemical properties and the in vivo behaviour. *Journal of Drug Targeting*, *10*, 221–230.

Munch, J. P., Candau, S., Herz, J., & Hild, G. (1977). Inelastic light scattering by gel modes in semi-dilute polymer solutions and permanent networks at equilibrium swollen state. *Journal of Physics (Paris)*, *38*, 971–976.

Provencher, S. W. (1982). A constrained regularization method for inverting data represented by linear algebraic or integral equations. *Computer Physics Communication*, *27*, 213–227.

Radosta, S., Haberer, M., & Vorwerg, W. (2001). Molecular characteristics of amylose and starch in dimethyl sulfoxide. *Biomacromolecules*, *2*, 970–978.

Ragheb, A. A., El-Sayiad, H. S., & Hebeish, A. (1997). Preparation and characterization of carboxymethyl starch (CMS) products and their utilization in textile printing. *Starch/Stärke*, *49*, 238–245.

Ring, S. G., I'Anson, K. J., & Morris, V. J. (1985). Static and dynamic light scattering studies of amylose solutions. *Macromolecules*, *18*, 182–188.

Roger, P., Bello-Perez, L. A., & Colonna, P. (1999). Contribution of amylose and amylopectin to the light scattering behaviour of starches in aqueous solution. *Polymer*, *40*(25), 6897–6909.

Roger, P., & Colonna, P. (1992). The influence of chain length on the hydrodynamic behaviour of amylose. *Carbohydrate Research*, *227*, 73–83.

Schaertl, W., & Roos, C. (1999). Convection and thermodiffusion of colloidal gold tracers by laser light scattering. *Physics Review E*, *60*, 2020–2028.

Schmidt, K. A., Herald, T. J., & Khatib, K. A. (2001). Modified wheat starches used as stabilizers in set-style yogurt. *Journal of Food Quality*, *24*, 421–434.

Schmitz, K. S. (1990). *An Introduction to dynamic light scattering by macromolecules*. San Diego: Academic Press.

Shibayama, M. (1998). Spatial inhomogeneity and dynamic fluctuations of polymer gels. *Macromolecular Chemistry and Physics*, *199*, 1–30.

Teraoka, I. (2002). *Polymer solutions: An introduction to physical properties*. New York: Wiley.

Viswanath, D. S., & Natarajan, G. (1989). *Data book on the viscosity of liquids*. New York: Hemisphere.

Wesslén, K. B., & Wesslén, B. (2002). Synthesis of amphiphilic amylose and starch derivatives. *Carbohydrate Polymers*, *47*, 303–311.

Whaley, J. K., Kasica, J. J., Senkeleski, J. L., Foss, J. W., Heigis, J. R. (1999). *Starch based hydrocolloid composition for use as a gelling agent viscosifier and stabilizer in food*. PCT International Applied WO, 9957996, 40pp.

Young, A. M., Brigault, C., Heenan, R., Higgins, J. S., & Peiffer, D. G. (1998). Small angle neutron scattering from ionomer gels. *Polymer*, *39*, 6685–6696.